Chapter 15
Optimal Planning of a Micro-combined Cooling, Heating and Power System Using Air-Source Heat Pumps for Residential Buildings

Farkhondeh Jabari, Behnam Mohammadi-Ivatloo and Mohammad Rasouli

Abstract This chapter explains a methodology for optimal planning of a micro-combined cooling, heating and power system driven by a solar dish Stirling heat engine. The solar dish concentrator collects the sun radiations and transforms them into thermal energy. The absorber and thermal storage systems are employed to absorb and store the thermal energy collected by a solar dish for continuous energy supplying when the sunlight is insufficient. The solar energy is absorbed and transferred to the working fluid in the hot point of the Stirling engine. The air source heat pump has been proposed to cool and heat the residential buildings in hot and cold weather conditions, respectively. During a hot weather, the air to air heat pump receives heat from the inside air and transfers it into the outside air, and vice versa in a cold climate. The heating energy obtained from air source heat pumps is not generated by a combustion process, rather it is transferred from the inside air to the outside air. Hence, the most promising aspect of the proposed micro-combined cooling, heating and power system is that it can be solar driven and transfer heat from the inside air during summer. Note that the process is reversed in winter times. Due to the increasing rate of carbon dioxide and more attention paid to the greenhouse gas emissions, use of solar energy and air source heat pumps in a micro-trigeneration system, which does not use any fossil fuel such as gasoline or natural gas, not only gives more chances to significant reduction of carbon dioxide, greenhouse gas emissions, and environmental pollution, but also increases the economic saving in fuel consumption. In an air to air heat pump, the electricity

F. Jabari · B. Mohammadi-Ivatloo (✉)
Faculty of Electrical and Computer Engineering, University of Tabriz, Tabriz, Iran
e-mail: bmohammadi@tabrizu.ac.ir

F. Jabari
e-mail: f.jabari@tabrizu.ac.ir

M. Rasouli
Department of Electrical and Computer Engineering, School of Engineering,
Penn State University, Erie, PA, USA
e-mail: mur37@psu.edu

N. Bizon et al. (eds.), *Energy Harvesting and Energy Efficiency*,
Lecture Notes in Energy 37, DOI 10.1007/978-3-319-49875-1_15

energy is only used by indoor/outdoor fans, and a compressor. Hence, the small-scale tri-generation system consumes less electrical energy than the traditional ones. In order to conduct an optimization, the mathematical model and thermodynamic analysis of proposed microsystem have been provided. Several key parameters related to solar dish Stirling heat engine and air to air heat pumps have been selected as the decision variables to minimize the cost of the electricity energy purchased from the main grid.

Abbreviation and Acronyms

AAHP	Air to Air Heat Pump
ASHP	Air Source Heat Pump
CCHP	Combined Cooling Heating and Power
CCP	Combined Cool and Power
CHP	Combined Heat and Power
CVaR	Conditional Value at Risk
DNLP	Discontinuous Nonlinear Program
GAMS	General Algebraic Modeling System
MILP	Mixed-Integer Linear Programming
ORC	Organic Rankine Cycle
SDSHE	Solar Dish Stirling Heat Engine
SOFC	Solid Oxide Fuel Cell
TVAC-PSO	Time Varying Acceleration Coefficients Particle Swarm Optimization
WAST	Warm Air Storage Tank

15.1 Introduction

In recent years, the urgent need to meet the increased power demand and to address the concerns over the environmental pollution as well as the greenhouse gas emissions reduction have led to employment of the tri-generation technology powered by renewable energy sources. The combined cooling, heating and power (CCHP) systems not only provide the cooling, heating and electricity demands of different customers such as residential, commercial and industrial loads, but also can provide reserve, peak saving and demand response services. As shown in Fig. 15.1, a typical tri-generation system consists of the following main components:

- Renewable energy sources such as solar, wind, hydroelectric energy, biomass, hydrogen and fuel cells, and geothermal power.
- Prime mover such as reciprocating internal combustion engine, combustion turbine, steam turbine, micro turbine, gas turbine, fuel cell, and Stirling engine as an external combustion engine.

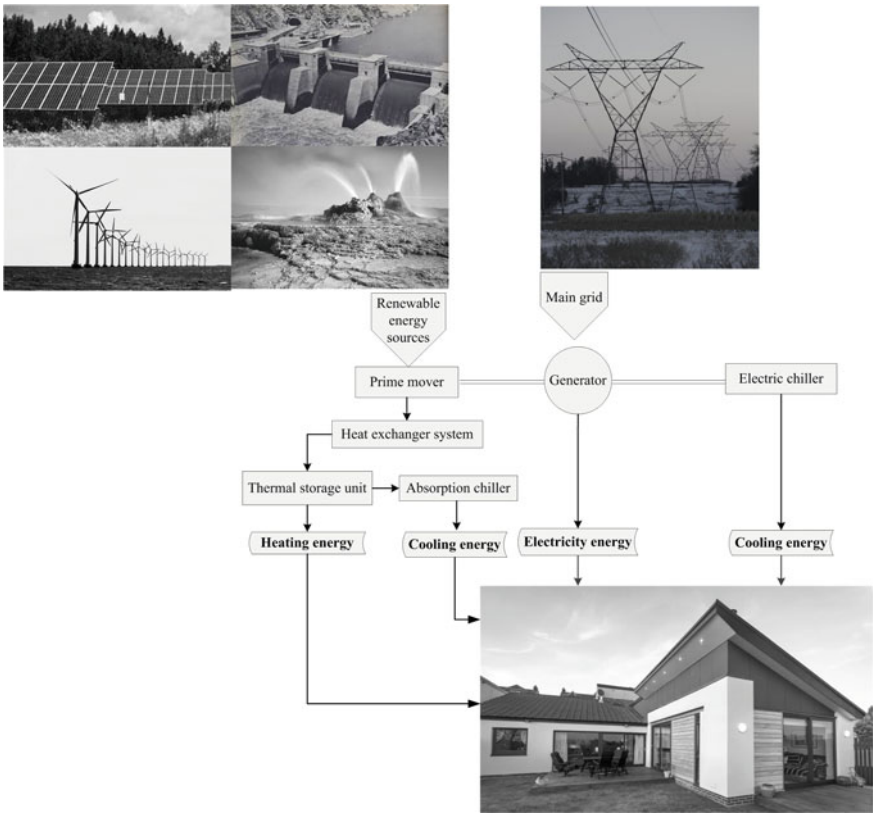

Fig. 15.1 Structure of a CCHP system

- Power generation unit.
- Electric chiller.
- Absorption chiller.
- Energy storage and thermal storage units.
- Electricity, cooling and heating loads.

Recently, several remarkable researches have been carried out to plan and evaluate a tri-generation system. In [1], a novel energy management strategy based on the variational electric cooling with combined electric and absorption chillers under unlimited and limited power generation unit capacity has been proposed. The variational electric cooling to cool load ratio has been optimized according to electric and thermal demands in every hour. In [2], a multi-objective optimization of a CCHP microgrid driven by solar energy has been investigated. The flat-plate solar collectors have been employed to collect the sun beam radiations and transform them into thermal energy. The heat storage system has been installed to store the collected thermal energy. Turbine inlet temperature, turbine inlet pressure, condensation temperature and pinch temperature difference in vapor generator have

been selected as the optimization decision variables to assess the performance of the entire solar CCHP microsystem. A two-stage optimal planning of tri-generation microgrid has been investigated in [3]. Total net present cost and carbon dioxide emission in life circle have simultaneously been minimized using non-dominated sorting genetic algorithm-II and mixed-integer linear programming (MILP) algorithm. In [4], exergoeconomic optimization of a CCHP system has been applied to maximize the total revenue requirement and the cost of the total system product using a genetic algorithm. Air compressor pressure ratio, gas turbine inlet temperature, pinch point temperatures in dual pressure heat recovery steam generator, pressure of the steam that enters the generator of the absorption chiller, process steam pressure and evaporator of the absorption chiller chilled water outlet temperature have been chosen as decision variables.

Reference [5] considers exergy modeling of a solar powered CCHP system consists of a single-effect absorption chiller, a heat exchanger, thermal storage tank, evaporator, absorber, solution expansion valve, solution pump, desorber, condenser, and organic Rankine cycle (ORC) components. Three operating conditions have been considered in this study: low solar radiation, high solar radiation, and storage mode in night. A real-time model of hydrogen tri-generation system and onsite hydrogen dispensing systems in the presence of price and market uncertainties has been developed in [6]. Application of two multi criteria decision-making algorithms denoted as fuzzy logic and the grey incidence methods are discussed in [7] to select the best prime mover for a residential tri-generation microgrid under five different climates. Technological, economic, environmental and social have been considered in the optimization process. Reference [8] introduces a novel CCHP system including a low temperature polymer electrolyte fuel cell and a desiccant wheel-based air handling unit. An integrated solid oxide fuel cell (SOFC) cogeneration micro-grid, fueled by coke oven gas that needs large amount of hydrogen is developed in [9]. Exhaust gas deep-recovery and thermoelectric generator based tri-generation system is presented in [10]. Thermoelectric generator and condenser are used to efficiently recover the exhaust gas waste heat of internal combustion engine. In [11], a small-scale solar tri-generation cycle combined with ORC has been proposed for hot and cold weather conditions. Turbine inlet temperature and pressure, turbine back pressure, evaporator temperature and heater outlet temperature are selected as the decision variables to improve thermal efficiency, exergy efficiency and total product cost rate. The proposed system could continuously and stably operate with installed thermal storage tank.

A novel CCHP microgrid with significant economic and environmental benefits, which consists of a power generation unit, an absorption chiller, two ground source heat pumps, a storage tank and two electric chillers has been introduced in [12]. The hourly programming with different cooling and heating demands has been carried out according to the outdoor climatic condition to improve system efficiency. In [13], a biomass tri-generation microgrid including a biomass gasifier, a heat pipe heat exchanger, an internal combustion engine, an absorption chiller and a heater for cooling and heating, and a heat exchanger to produce domestic hot water has been proposed. Operational planning has been provided in three modes: summer,

winter, and the transient seasons. In [14], a novel micro-CCHP equipped with 20 kW Lombardini diesel engine and a double effect water-LiBr absorption chiller has been introduced to generate hot water, by recovering heat from the engine cooling system, and chilled water, by recovering heat from the engine exhaust gasses. The engine and the absorption chiller have been modeled by means of 0–1D dimensional and thermochemical models, respectively. A Honda gas engine based micro-CCHP, which utilizes a heat recovery system, has been proposed to satisfy the required heating, cooling and electrical energy of a residential building according to the air conditions [15]. The formulation of a CCHP system including an air-conditioning system and a heat storage tank in residential and office buildings in Dalian, China is presented in [16]. The energy saving, total cost, and environmental pollution reduction have been considered as main objectives in the genetic based optimization process. In [17], a small scale CCHP system has been introduced. The waste heat of internal combustion engine is collected and managed using a thermal management controller. The waste heat can be used for heating or cooling cycle. The part load ratio of the internal combustion engine, buffer tank set point temperature, hot water tank set point temperature, chilled water temperature and cooling water temperature of adsorption chiller are treated as decision variables. Thermal management controller is used to manage the waste heat. The heating output of the thermal management controller is regulated via buffer tank and hot water tank set point temperatures. A CCHP microgrid with a gas turbine, a heat recovery steam generator unit and an absorption heat pump driven by a steam turbine has been designed in [18]. Genetic algorithm is used to minimize the total annual cost and maximize the exergy efficiency. In [19], a reliable grassroots biomass based cogeneration system has been designed according to the equipment redundancy. Chance constrained programming and k-out-of-m system modeling have been applied to solve a multi period optimization process.

A tri-generation system including a solid oxide fuel cell, an air pre-heater, an ethanol reformer, a steam generator and a double-effect $LiBr/H_2O$ absorption chiller, which uses the heat recovery of the solid oxide fuel cell exhaust gas, has been proposed in [20]. In order to evaluate the performance of the presented microgrid, a parametric assessment of the effects of the current density, solid oxide fuel cell temperature, fuel consumption ratio and solid oxide fuel cell anode recirculation ratio variations on total net electrical, heating and cooling energies have been provided. An energy management strategy has been proposed to increase the biomass-CCHP yearly efficiency by managing the output heating energy [21], where double piping district heating and cooling demands of a residential building have been considered. In the maximization process of the net present value, hourly heating and cooling load have been forecasted using the degree-hour method. Energy and exergy based management of a three-reactor chemical looping hydrogen generation process of a zero emission tri-generation plant has been presented in [22]. The proposed tri-generation microsystem involves an air separation unit, gasification unit, a chemical looping hydrogen generation system, an extended heat recovery steam generation unit, an ORC and space heating, a two-stage steam Rankine cycle with reheat and regenerator and an ORC. The optimal energy

management in energy hubs has recently attracted a great deal of attention around the world. The energy hub consists of several inputs (energy resources) and outputs (energy consumptions) and also some energy conversion/storage devices. The energy hub can be a home, large consumer, power plant, etc. The objective is to minimize the energy procurement costs (fuel/electricity/environmental aspects) subject to a set of technical constraints. In [23], a comprehensive multi-objective model is proposed to minimize both the energy procurement cost and risk level in energy hub. For controlling the pernicious effects of the uncertainties, conditional value at risk (CVaR) is used as risk management tool. A novel time varying acceleration coefficients particle swarm optimization (TVAC-PSO) algorithm is implemented to solve combined heat and power economic dispatch problem in [24].

To achieve a practical planning of CCHP microgrids with no combustion process and no emission of potentially dangerous gases, high economic and technological efficiency are difficult challenges to be addressed. In the literature, remarkable efforts have been made to manage on the energy and exergy of tri-generation systems. However, some problems have not been resolved yet. Among those are the significant reduction of the greenhouse gas emissions and the risk of the environmental pollutants, reducing the fossil fuel consumption using renewable energy sources, and economic savings due to energy exchanges with the main grid. This chapter develops an hourly scheduling of a novel micro tri-generation system to satisfy the electrical, heating and cooling demands of a residential building. A solar dish Stirling heat engine (SDSHE) is used as the prime mover to provide the required input mechanical power for the power generation unit. Thus, there is no need for a combustion process, fossil fuel consumption or equipment in the combustion process such as a combustion chamber, an air compressor and a gas turbine. Therefore, there will be no greenhouse gas emissions involved. The proposed small-scale CCHP system is designed to operate in two different modes:

- Combined heat and power (CHP) mode based on the heating cycle of the air to air heat pump (AAHP) in the cold weather.
- Combined cool and power (CCP) mode based on the refrigeration cycle of the air to air heat pump on hot days.

The electric chiller is also used to supply a part of the required cold energy in the cooling mode. Furthermore, the proposed air to air heat pump based small-scale CCHP microgrid has the following advantages:

- Air to air heat pumps can provide cooling energy in hot climate condition, and vice versa.
- Air to air heat pumps requires less maintenance than the combustion process based heating systems.
- Similar to the SDSHE, air to air heat pumps are safe. No combustion or emission is involved.

- Air to air heat pumps save carbon emissions. Unlike the burning oil, gas, and biomass, an air to air heat pump produces no carbon emissions on site (no greenhouse gas emissions at all, if a renewable source of electricity such as solar or wind is used to power them).
- Air to air heat pumps are cheaper to run than the oil boilers and can be cheaper than the running gas boilers.

The remainder of this chapter is organized as follows: Sect. 15.2 expresses the basic concepts related to the solar powered Stirling heat engine and the refrigeration cycle of the air source heat pumps. The energy and the exergy of the proposed micro-combined cooling, heating and power system are analyzed in Sect. 15.3. Simulation results and discussions are presented in Sect. 15.4. Finally, Sect. 15.5 concludes the chapter.

15.2 Proposed Small-Scale Tri-generation System for Residential Buildings

15.2.1 Solar Dish Stirling Heat Engine (SDSHE)

In this chapter, the solar energy is used as a renewable energy source to drive a Stirling engine, which is used to supply the primary mechanical power required for a power generation unit [25]. The location of an absorber and a thermal storage unit on a solar-dish concentrator are illustrated in Fig. 15.2.

As shown in Fig. 15.3, the Stirling cycle comprises of four processes. Process 1–2 is an isothermal process, in which the working fluid after compressing at constant temperature T_c and rejected heat to the heat sink at low temperature T_{L_1}, the temperature of heat sink is increased to T_{L_2}. Then, the working fluid crosses over the regenerator and warms up to T_h in an isochoric process 2–3. In process 3–4, the working fluid is expanded in a constant temperature T_h process and receives heat from the heat source in which its temperature is reduced from T_{H_1} to T_{H_2}. Last process (4–1), is an isochoric cooling process, where the regenerator absorbs heat from the working fluid.

The actual useful heat gain of the dish collector, q_u, considering the conduction, convection and radiation losses can be obtained as [25]:

$$q_u = IA_{app}\eta_0 - A_{rec}[h(T_{H_{ave}} - T_0) + \varepsilon\delta(T_{H_{ave}}^4 - T_0^4)] \tag{15.1}$$

where:

I Direct solar flux intensity in $\mathrm{W} \cdot \mathrm{m}^{-2}$
A_{app} Collector aperture area in m^2
η_0 Collector optical efficiency
A_{rec} Absorber area in m^2

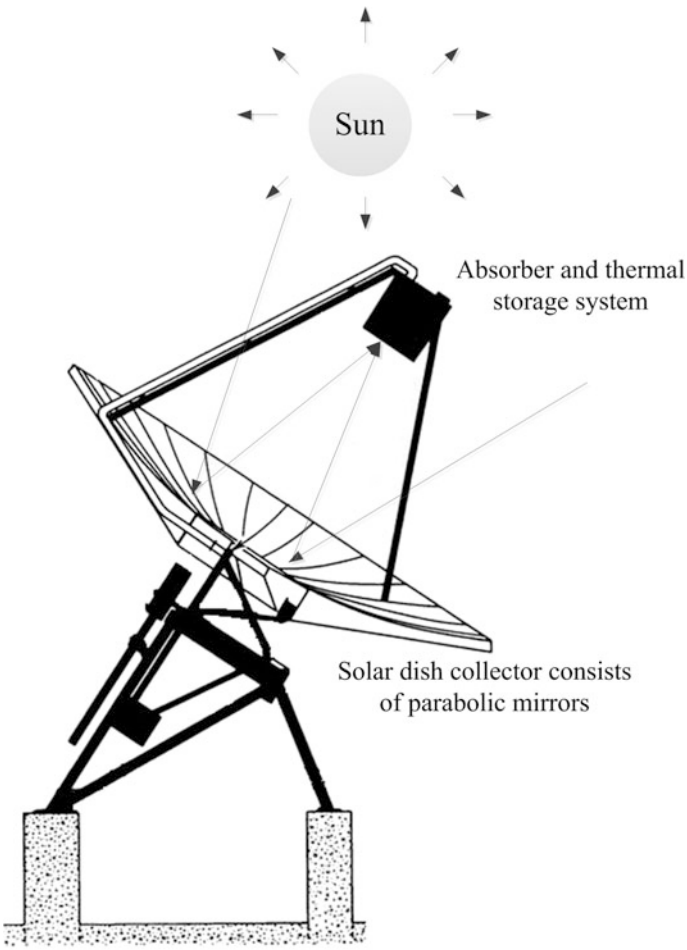

Fig. 15.2 The location of an absorber and a thermal storage unit on a solar-dish concentrator

h Conduction-convection heat transfer coefficient in $W \cdot m^{-2} \cdot K^{-1}$
$T_{H_{ave}}$ Average absorber temperature in K
T_0 Ambient temperature in K
ε Effectiveness factor of collector
δ Stefan's constant in $W \cdot m^{-2} \cdot K^{-4}$

Thermal efficiency of the dish collector, η_s is calculated from:

$$\eta_s = \frac{q_u}{IA_{app}} = \eta_0 - \frac{h(T_{H_{ave}} - T_0) + \varepsilon\delta(T_{H_{ave}}^4 - T_0^4)}{IC} \tag{15.2}$$

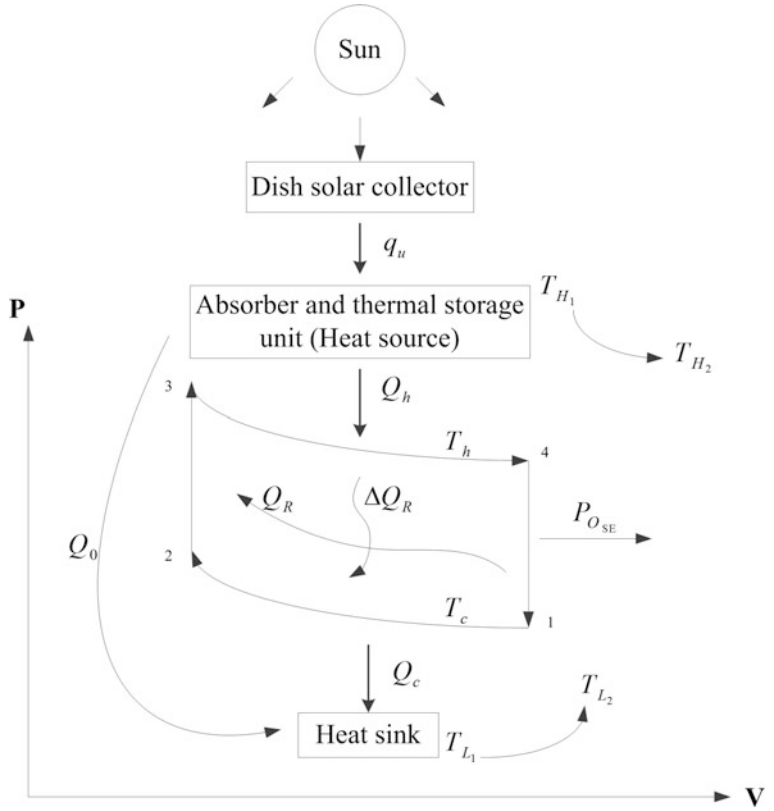

Fig. 15.3 Stirling cycle of a solar dish Stirling heat engine [23]

where, C is heat capacitance rate in $\mathrm{W} \cdot \mathrm{K}^{-1}$. The regenerative heat transfer and the heat loss during two regenerative processes are given by following equations:

$$Q_R = nC_v\varepsilon_R(T_h - T_c) \tag{15.3}$$

$$\Delta Q_R = nC_v(1 - \varepsilon_R)(T_h - T_c) \tag{15.4}$$

where:

Q_R Regenerative heat transfer in J
n Number of moles
C_v Specific heat capacity in $\mathrm{J} \cdot \mathrm{mol}^{-1} \cdot \mathrm{K}^{-1}$
ε_R Effectiveness of regenerator
T_h Working fluid temperature in the hot space in K
T_c Working fluid temperature in the cold space in K
ΔQ_R Heat loss during two regenerative processes in the cycle in J

The temperature of the working fluid in the regenerative processes can be calculated as follows:

$$\frac{dT}{dt} = \pm M_i \tag{15.5}$$

where, M is the regenerative time constant in $\mathrm{K} \cdot \mathrm{s}^{-1}$. The positive and negative signs are considered for the heating and cooling processes, respectively. The times of the two isochoric heating ($i = 1$) and cooling ($i = 2$) processes are calculated according to (15.6) and (15.7), respectively.

$$t_3 = \frac{T_1 - T_2}{M_1} \tag{15.6}$$

$$t_4 = \frac{T_1 - T_2}{M_2} \tag{15.7}$$

The heat released between the heat source and the working fluid and the heat absorbed between the working fluid and the heat sink are given by (15.8) and (15.9), respectively [25].

$$\begin{aligned} Q_h &= nRT_h \ln \lambda + nC_v(1 - \varepsilon_R)(T_h - T_c) \\ &= t_h\left[C_H \varepsilon_H (T_{H_1} - T_h) + \xi C_H \varepsilon_H (T_{H_1}^4 - T_h^4)\right] \end{aligned} \tag{15.8}$$

$$Q_c = nRT_c \ln \lambda + nC_v(1 - \varepsilon_R)(T_h - T_c) = t_l C_L \varepsilon_L (T_c - T_{L_1}) \tag{15.9}$$

where:

Q_h Heat released between the heat source and the working fluid in J
R Gas constant in $\mathrm{J} \cdot \mathrm{mol}^{-1} \cdot \mathrm{K}^{-1}$
λ Ratio of volume during the regenerative processes
t_h Heat exchanging time at heat source in s
C_H Heat capacitance rate of the heat source in $\mathrm{W} \cdot \mathrm{K}^{-1}$
ε_H Effectiveness of the high temperature heat exchanger
T_{H_1} Primary heat source temperature in K
Q_c Heat absorbed between the working fluid and the heat sink in J
t_l Heat exchanging time of the heat sink in s
C_L Heat capacitance rate of the heat sink in $\mathrm{W} \cdot \mathrm{K}^{-1}$
ε_L Effectiveness of the low temperature heat exchanger
T_{L_1} Primary heat sink temperature in K

The cyclic period of the SDSHE can be calculated from [25]:

$$t = \frac{nRT_h \ln\lambda + nC_v(1-\varepsilon_R)(T_h - T_c)}{C_H\varepsilon_H(T_{H_1} - T_h) + \xi C_H\varepsilon_H(T_{H_1}^4 - T_h^4)} + \frac{nRT_h \ln\lambda + nC_v(1-\varepsilon_R)(T_h - T_c)}{C_L\varepsilon_L(T_c - T_{L_1})} + (\frac{1}{M_1} + \frac{1}{M_2})(T_h - T_c) \tag{15.10}$$

where, t is the cyclic period in s. The conductive thermal losses from the heat source to the heat sink can be obtained from the following equations:

$$Q_0 = tK_0(T_{H_{ave}} - T_{L_{ave}}) \tag{15.11}$$

$$T_{H_{ave}} = \frac{T_{H_1} + T_{H_2}}{2} \tag{15.12}$$

$$T_{L_{ave}} = \frac{T_{L_1} + T_{L_2}}{2} \tag{15.13}$$

in which:

Q_0 Conductive thermal losses in J
K_0 Heat leak coefficient in $\mathrm{W \cdot K^{-1}}$
$T_{H_{ave}}$ Heat source average temperature in K
T_{H_2} Secondary heat source temperature in K
$T_{L_{ave}}$ Heat sink average temperature in K
T_{L_2} Secondary heat sink temperature in K

Note that:

$$T_{H_2} = (1-\varepsilon_H)T_{H_1} + \varepsilon_H T_h \tag{15.14}$$

$$T_{L_2} = (1-\varepsilon_L)T_{L_1} + \varepsilon_L T_c \tag{15.15}$$

Hence,

$$Q_0 = \frac{K_0}{2}t[T_{H_1}(2-\varepsilon_H) - T_{L_1}(2-\varepsilon_L) + \varepsilon_H T_h - \varepsilon_L T_c] \tag{15.16}$$

The net heat released from the heat source and the net heat absorbed by the heat sink can be obtained from (15.17) and (15.18), respectively.

$$Q_H = Q_h + Q_0 \tag{15.17}$$

$$Q_L = Q_c + Q_0 \tag{15.18}$$

where:

Q_H Net heat released from the heat source in J
Q_L Net heat absorbed by the heat sink in J

The output power of the SDSHE is given by (15.19) [25]:

$$\begin{aligned} P_{O_{\mathrm{SE}}} &= \frac{nR\ \ln\lambda(T_h - T_c)}{F_1 + F_2 + F_3} \\ F_1 &= \frac{nRT_h \ln\lambda + nC_v(1-\varepsilon_R)(T_h - T_c)}{C_H\varepsilon_H(T_{H_1} - T_h) + \xi C_H\varepsilon_H(T_{H_1}^4 - T_h^4)} \\ F_2 &= \frac{nRT_h \ln\lambda + nC_v(1-\varepsilon_R)(T_h - T_c)}{C_L\varepsilon_L(T_c - T_{L_1})} \\ F_3 &= (\frac{1}{M_1} + \frac{1}{M_2})(T_h - T_c) \end{aligned} \tag{15.19}$$

In (15.19), $P_{O_{\mathrm{SE}}}$ is the output power in kW.

15.2.2 Air Source Heat Pumps (ASHPs)

An air source heat pump is an electrical device that extracts heat from the inside air and transfers it to the outside air in hot climate and vice versa in cold weather [26]. In other words, the air source heat pump's cycle is reversible. Based on the heating and the cooling energy exchange sources, the air source heat pumps can be classified in two general categories:

- Air to water heat pump
  The first type is the air to water heat pump. In cold weather, it absorbs heat from the outside air and transfers it to the water in the hydronic distribution unit. In hot weather conditions, it extracts heat from the water in the hydronic distribution unit and pumps it to the outside air.
- Air to air heat pump (AAHP)
  The most common type of the air source heat pumps is the air to air heat pump. An AAHP extracts heat from the air and transfers it to the inside or the outside air of the building depending on the season. There are two cycles for an air source heat pump: The cooling cycle and the heating cycle.

15.2.2.1 The Cooling Cycle of the Air to Air Heat Pump

The cooling cycle of the building using the air to air heat pump is shown in Fig. 15.4. In the cooling process of the building inside space, the heating energy is taken from the indoor air and then pumped to the outdoor air. An AAHP contains the following component: compressor, evaporator, condenser, and an expansion valve. The liquid refrigerant enters the indoor evaporator coils. In the inside evaporator, the low pressure liquid refrigerant absorbs heat from the warm inside air, vaporizes, and changes into a low temperature or cold vapor. The compressor coil then pumps the vapor, increases its pressure, and changes it into a hot high pressure vapor. The generated high-temperature high-pressure vapor passes over the condenser coil and then heating energy is given off to the outside air, and the vapor condenses to change to a high-temperature high-pressure liquid. The generated liquid then passes over the expansion valve and changes into the low-temperature low-pressure liquid refrigerant. The cooling cycle is then repeated again. The energy required to operate the cooling cycle is the electrical energy, which powers the compressor inside and outside fans.

15.2.2.2 The Heating Cycle of the Air to Air Heat Pump

In the heating process, the heating flow is taken from the outdoor cold air and then pumped to the inside cold air. The outside air always contains some heat, a heat pump can supply heat to a building even on cold days [26]. The heating process of the residential buildings using the AAHPs is shown in Fig. 15.5.

During the heating process, the liquid refrigerant enters the outdoor evaporator coil and absorbs heat from the outdoor air to evaporate, and changes into the low temperature liquid and vapor mixture. The vapor then enters the compressor, compressed, changes into the high temperature high pressure vapor. The heating

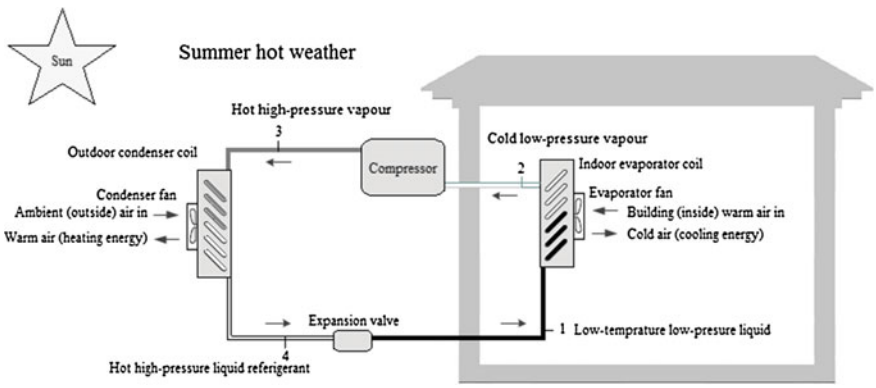

Fig. 15.4 The cooling cycle of the building using the air to air heat pump

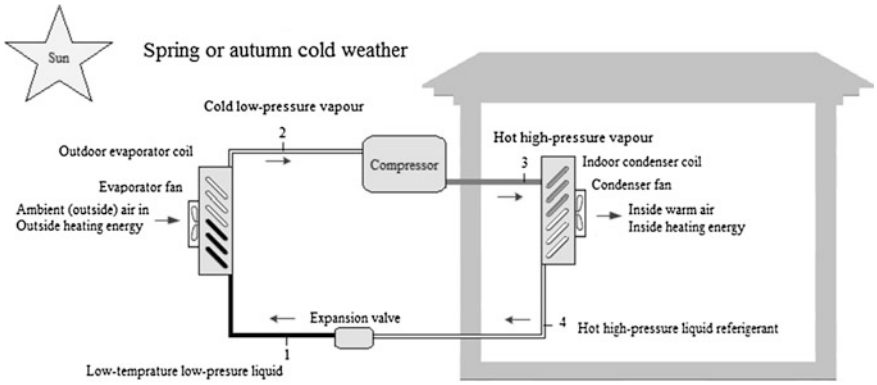

Fig. 15.5 The heating cycle of the building using the air to air heat pump

energy from the high temperature high pressure vapor is transferred to the inside cold air, causing the refrigerant to condense into the high temperature high pressure liquid. The hot high pressure liquid passes though the expansion valve and changes into the low temperature low pressure liquid refrigerant. Similar to the cooling cycle, the electrical energy powers the compressor, the inside and the outside fans.

15.3 Energy and Exergy Analysis of the Proposed Micro Tri-generation System

15.3.1 Combined Cooling and Power (CCP) Mode for Hot Weather Conditions

The CCP mode of the proposed micro-CCHP system, which can be used for residential buildings, is shown in Fig. 15.6. According to Fig. 15.6, the SDSHE is used to drive the power generation unit. The output electric power generated by the power generating unit can be obtained from (15.20):

$$P_{PGU} = \eta_{elec} P_{O_{SE}} \tag{15.20}$$

where, P_{PGU} is the output electric power in kW and η_{elec} is the electrical efficiency of the power generating unit. The cooling energy generated by an AAHP, Q_{evap}, can be calculated from the following equation:

$$Q_{evap} = \dot{m}_4 (h_1 - h_4) \tag{15.21}$$

where, Q_{evap} and $\dot{m}_4$ are the cooling energy generated by the AAHP in kW, and the mass flow rate of the refrigerant through each component such as evaporator, compressor, condenser and expansion valve in kg $\cdot$ s^{-1}, respectively. Variables h_1 and h_4

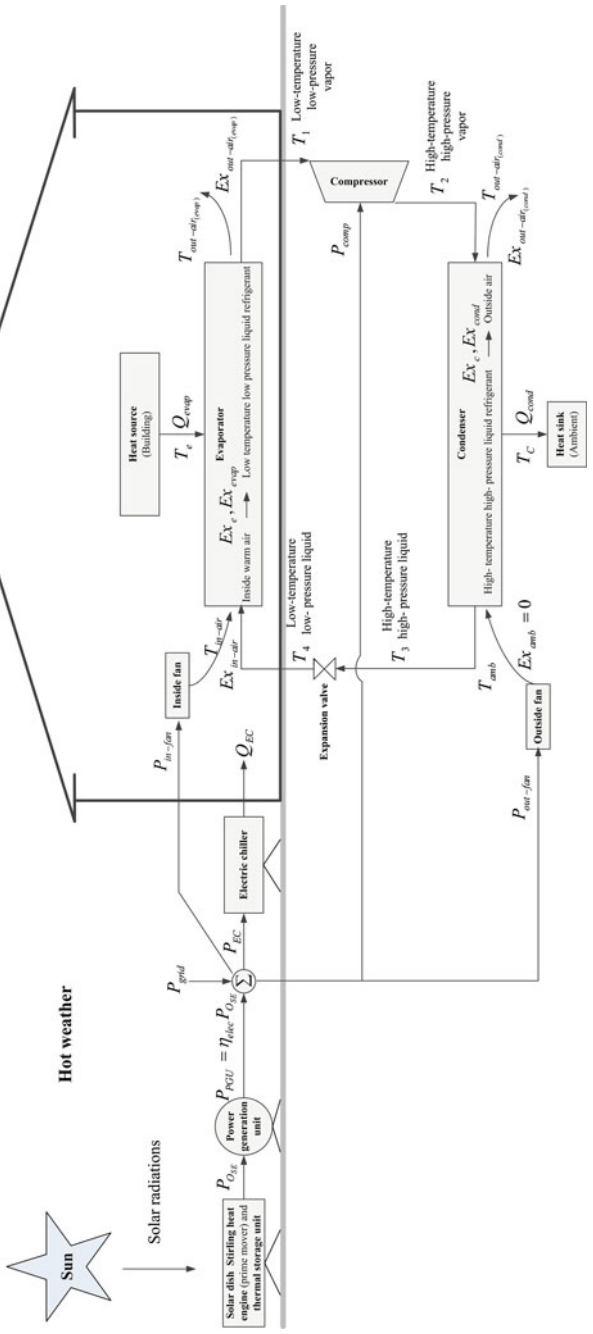

Fig. 15.6 The schematic of the proposed micro tri-generation system in CCP mode

are the rate of heat transfer per unit mass in $kJ \cdot kg^{-1}$ in the states 1 and 4, respectively. As (15.22), the electric energy consumed by the electric chiller can be calculated according to the coefficient of performance and its output cooling energy, that is:

$$P_{EC} = \frac{Q_{EC}}{COP} \tag{15.22}$$

where, Q_{EC} is the output cooling energy generated by the electric chiller, which can be obtained from (15.23):

$$Q_{EC} = Q_{Cool} - Q_{evap} \tag{15.23}$$

The Q_{Cool} is the cooling demand in a residential building in kW. The electric energy consumed by the indoor fan is given by:

$$P_{in-fan} = C_a m_{in-air}(T_{out-air_{evap}} - T_{in-air}) + Q_{evap} \tag{15.24}$$

where:

P_{in-fan}	Electric energy consumed by indoor fan in kW
C_a	Specific heat capacity of air in $kJ \cdot kg^{-1} \cdot K^{-1}$
m_{in-air}	Airflow rate of the inside fan in $kg \cdot s^{-1}$
$T_{out-air_{evap}}$	Chilled inside air temperature in K
T_{in-air}	Indoor air temperature in K

The consumed and the transferred exergy at the evaporator can be computed from (15.25)–(15.29):

$$Ex_{in-air} = C_a m_{in-air}\left[(T_{in-air} - T_{amb}) - T_{amb}\ln\left(\frac{T_{in-air}}{T_{amb}}\right)\right] \tag{15.25}$$

$$Ex_{out-air_{evap}} = C_a m_{in-air}\left[(T_{out-air_{evap}} - T_{amb}) - T_{amb}\ln\left(\frac{T_{out-air_{evap}}}{T_{amb}}\right)\right] \tag{15.26}$$

$$S_{evap} = C_a m_{in-air}\ln\left(\frac{T_{out-air_{evap}}}{T_{in-air}}\right) + \frac{Q_{evap}}{T_e} \tag{15.27}$$

$$Ex_{evap} = S_{evap} T_{amb} \tag{15.28}$$

$$P_{in-fan} + Ex_e - Ex_{evap} = Ex_{out-air_{evap}} - Ex_{in-air} \tag{15.29}$$

where:

Ex_{in-air}	Indoor air exergy in kW
T_{amb}	Ambient temperature in K
$Ex_{out-air_{evap}}$	Supplied inside air exergy in kW

S_{evap} Entropy generated in the heat exchanging process between indoor air and the refrigerant in $kW \cdot K^{-1}$

Ex_{evap} Exergy consumed in the heat exchanging process between the indoor air and the refrigerant at the evaporator in kW

Ex_e Exergy transferred from the indoor air to the refrigerant at the evaporator in kW

The electric energy consumed by the outdoor fan can be determined from Eqs. (15.30)–(15.34):

$$Q_{cond} = \dot{m}_2(h_2 - h_3) \tag{15.30}$$

$$Ex_c = Q_{cond}\left(\frac{T_C - T_{amb}}{T_C}\right) \tag{15.31}$$

$$S_{cond} = C_a m_{out-air} \ln\left(\frac{T_{out-air_{cond}}}{T_{amb}}\right) - \frac{Q_{cond}}{T_C} \tag{15.32}$$

$$Ex_{cond} = S_{cond} T_{amb} \tag{15.33}$$

$$P_{out-fan} + Ex_c - Ex_{cond} = Ex_{out-air_{cond}} - Ex_{amb} \tag{15.34}$$

where:

Q_{cond} Energy flux between refrigerant and outdoor air in kW

$\dot{m}_2$ Mass flow rate of refrigerant through each component such as evaporator, compressor, condenser and expansion valve in $kg \cdot s^{-1}$

h_2, h_3 Rate of heat transfer per unit mass in $kJ\,kg^{-1}$ in states 2 and 3, respectively

Ex_c Exergy transferred from the refrigerant to the outdoor air in kW

T_C Refrigerant condensation temperature in K

S_{cond} Entropy generated in the heat exchanging process between the outdoor air and the refrigerant in $kW \cdot K^{-1}$

Ex_{cond} Exergy consumed between the outdoor air and refrigerant in kW

$P_{out-fan}$ Electric energy consumed by the outdoor fan in kW

Ex_{amb} Ambient air exergy (=0) in kW

$Ex_{out-air_{cond}}$ Outlet air exergy of the outdoor fan in kW, which can be calculated from (15.35):

$$Ex_{out-air_{cond}} = C_a m_{out-air}\left[(T_{out-air_{cond}} - T_{amb}) - T_{amb} \ln\left(\frac{T_{out-air_{cond}}}{T_{amb}}\right)\right] \tag{15.35}$$

where:

$m_{out-air}$ Airflow rate of outside fan in $kg \cdot s^{-1}$

$T_{out-air_{cond}}$ Supplied outside air temperature in K

The electric energy consumed by the compressor can be obtained using (15.36) and (15.38):

$$S_{cycle} = \frac{Q_{cond}}{T_3} - \frac{Q_{evap}}{T_1} \tag{15.36}$$

$$Ex_{cycle} = S_{cycle} T_{amb} \tag{15.37}$$

$$P_{comp} = Ex_c + Ex_e + Ex_{cycle} \tag{15.38}$$

where:

S_{cycle} Entropy generated in the refrigerant cycle in $kW \cdot K^{-1}$
Ex_{cycle} Exergy consumed in the refrigerant cycle in kW
P_{comp} Electric energy consumed by the compressor in kW

The electricity energy need to be purchased from the main grid, and can be computed from the following energy balance equation:

$$P_{grid} = (P_{comp} + P_{in-fan} + P_{out-fan}) + P_{EC} + P_{demand} - P_{PGU} \tag{15.39}$$

where, P_{grid} and P_{demand} are the electricity energy purchased from the local network and the electrical demand in the residential building, respectively in kW.

15.3.2 Combined Heating and Power (CHP) Mode for Cold Weather Condition

The combined heating and power mode of the proposed micro CCHP system for residential applications is depicted in Fig. 15.7. The heating energy generated by the AAHP, Q_{cond}, can be calculated from (15.30). The electric energy consumed by the outdoor fan is given by Eq. (15.40).

$$P_{out-fan} = C_a m_{out-air} (T_{out-air_{evap}} - T_{amb}) + Q_{evap} \tag{15.40}$$

where, $T_{out-air_{evap}}$ is the chilled outside air temperature in K. The consumed and the transferred exergy at the evaporator can be calculated attained from Eqs. (15.28) and (15.41)–(15.43):

$$S_{evap} = C_a m_{out-air} \ln\left(\frac{T_{out-air_{evap}}}{T_{amb}}\right) + \frac{Q_{evap}}{T_e} \tag{15.41}$$

$$Ex_{out-air_{evap}} = C_a m_{out-air} \left[(T_{out-air_{evap}} - T_{amb}) - T_{amb} \ln\left(\frac{T_{out-air_{evap}}}{T_{amb}}\right)\right] \tag{15.42}$$

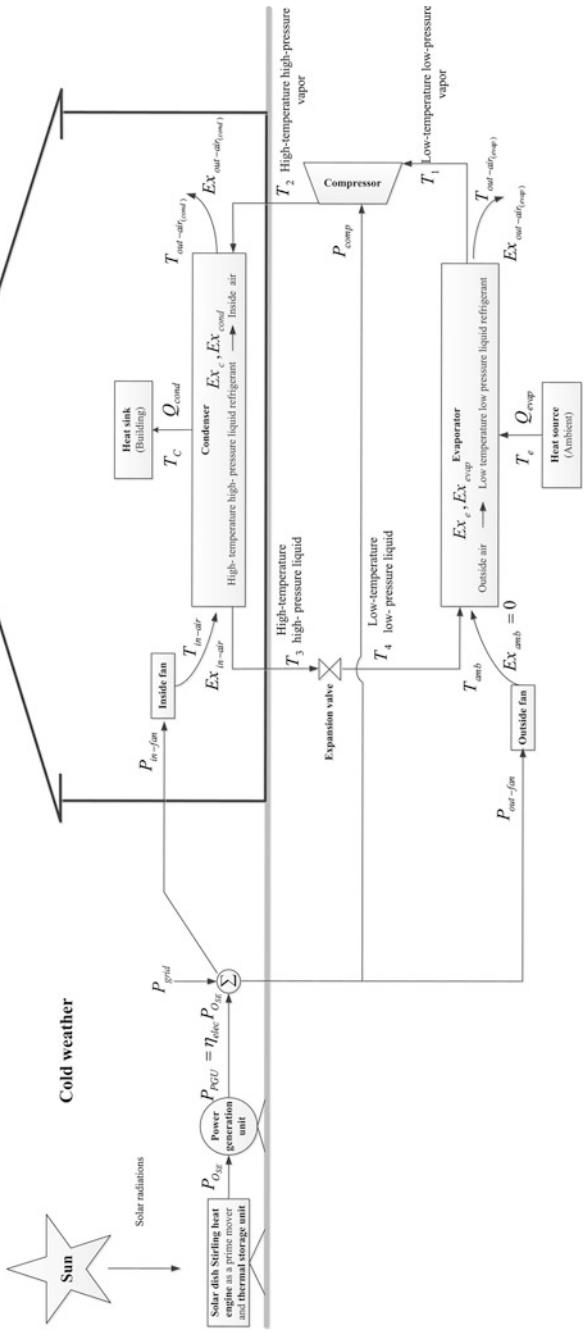

Fig. 15.7 The schematic of the proposed micro-CCHP system in CHP mode

$$P_{out-fan} + Ex_e - Ex_{evap} = Ex_{out-air_{evap}} - Ex_{amb} \tag{15.43}$$

where:

S_{evap} Entropy generated in the heat exchanging process between outdoor air and the refrigerant in $\text{kW} \cdot \text{K}^{-1}$

$Ex_{out-air_{evap}}$ Supplied outside air exergy in kW

Ex_{evap} Exergy consumed in the heat exchanging process between the outdoor air and the refrigerant at the evaporator in kW

Ex_e Exergy transferred from the outdoor air to the refrigerant at the evaporator in kW

The consumed and the transferred exergy at the condenser can be calculated from Eqs. (15.25), (15.33) and (15.44)–(15.46):

$$S_{cond} = C_a m_{in-air} \ln\left(\frac{T_{out-air_{cond}}}{T_{in-air}}\right) - \frac{Q_{cond}}{T_C} \tag{15.44}$$

$$Ex_{out-air_{cond}} = C_a m_{in-air}\left[(T_{out-air_{cond}} - T_{amb}) - T_{amb} \ln\left(\frac{T_{out-air_{cond}}}{T_{amb}}\right)\right] \tag{15.45}$$

$$P_{in-fan} + Ex_c - Ex_{cond} = Ex_{out-air_{cond}} - Ex_{in-air} \tag{15.46}$$

where:

$Ex_{out-air_{cond}}$ Outlet air exergy of indoor fan in kW

$T_{out-air_{cond}}$ Supplied inside air temperature in K

Similar to the cooling process, the electric energy consumed by the compressor can be obtained from (15.36)–(15.38).

15.3.3 Optimization Problem Formulation

The following objective function is considered to minimize the total hourly energy cost purchased from the main network:

$$\text{Objective} = Min\{\lambda_t P^t_{grid}\} \tag{15.47}$$

where, λ_t is the energy price at time t in $\$ \cdot \text{kW}^{-1}\text{h}^{-1}$. In the optimization process, C_H, C_L, T_h, T_c, $T_{out-air_{cond}}$, $T_{out-air_{evap}}$ (For CHP mode) are the decision variables. The optimization constraints for finding optimal operating scenario can be summarized as follows:

$$300 < C_H < 2000 \tag{15.48}$$

$$300 < C_L < 2000 \tag{15.49}$$

$$800 < T_h < 1200\,\mathrm{K} \tag{15.50}$$

$$400 < T_c < 710\,\mathrm{K} \tag{15.51}$$

$$P_{comp} > 0 \tag{15.52}$$

$$P_{in-fan} > 0 \tag{15.53}$$

$$P_{out-fan} > 0 \tag{15.54}$$

$$Ex_{out-air_{evap}} > 0 \tag{15.55}$$

$$Ex_e > 0 \tag{15.56}$$

$$Ex_{out-air_{cond}} > 0 \tag{15.57}$$

$$T_{in-air} < T_{amb} \quad \text{for CCP mode} \tag{15.58}$$

$$T_{out-air_{cond}} > T_{amb} \exp\left(\frac{Q_{cond}}{C_a m_{out-air} T_c}\right) \quad \text{for CCP mode} \tag{15.59}$$

$$T_{in-air} > T_{amb} \quad \text{for CHP mode} \tag{15.60}$$

$$T_{out-air_{evap}} > Max\left\{T_{amb} \exp\left(\frac{-Q_{evap}}{C_a m_{out-air} T_e}\right), \left(\frac{-Q_{evap}}{C_a m_{out-air}} + T_{amb}\right)\right\} \quad \text{for CHP mode} \tag{15.61}$$

$$T_{out-air_{evap}} = 292\,\mathrm{K}\ (19\,^{\circ}\mathrm{C}) \quad \text{for CCP mode} \tag{15.62}$$

$$T_{out-air_{cond}} > 180\,^{\circ}\mathrm{F}\,(355.22\,\mathrm{K}) \quad \text{for CHP mode} \tag{15.63}$$

$$P_{grid} < P_{grid}^{\max} \tag{15.64}$$

15.4 Simulation Results and Discussion

In order to achieve the optimal performance of the proposed micro tri-generation system, the optimization process is conducted in two typical conditions: hot weather (CCP mode), and cold weather (CHP mode). A discontinuous nonlinear program (DNLP) is solved using CONOPT solver under general algebraic modeling system (GAMS) optimization software. The required parameters for the simulation of the solar micro-CCHP system are listed at appendix. In this chapter,

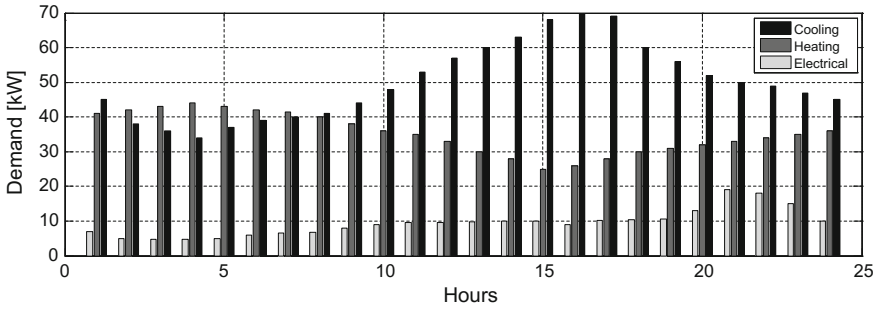

Fig. 15.8 Cooling, heating and electrical demands of test building located in Tabriz, Iran [27]

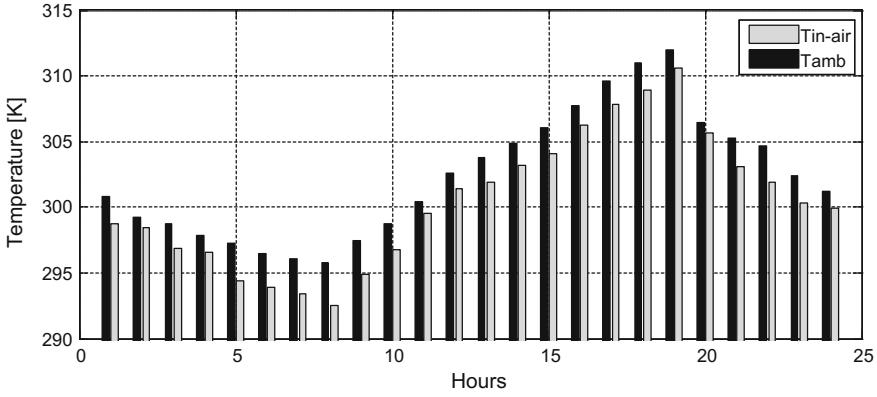

Fig. 15.9 The ambient and the indoor air temperatures during a sample hot day in Tabriz, Iran

the mass flow rate of the refrigerant, and the specific heat capacity of air are assumed to be constant due to the negligible changes during a hot or cold day. A benchmark residential building is considered in Tabriz, Iran to demonstrate the robustness and the effectiveness of the proposed CCHP system. The cooling, heating and electrical demands are shown in Fig. 15.8.

15.4.1 CCP Mode

The variations of the ambient and the indoor air temperatures during a sample summer day is depicted in Fig. 15.9.

The obtained optimal operating points of the proposed micro-CCHP system during the typical summer day are reported in Figs. 15.10, 15.11 and Table 15.1.

As shown in Fig. 15.11, the output mechanical power of the SDSHE increases monotonically as the sum of the electric energy consumed by compressor, inside

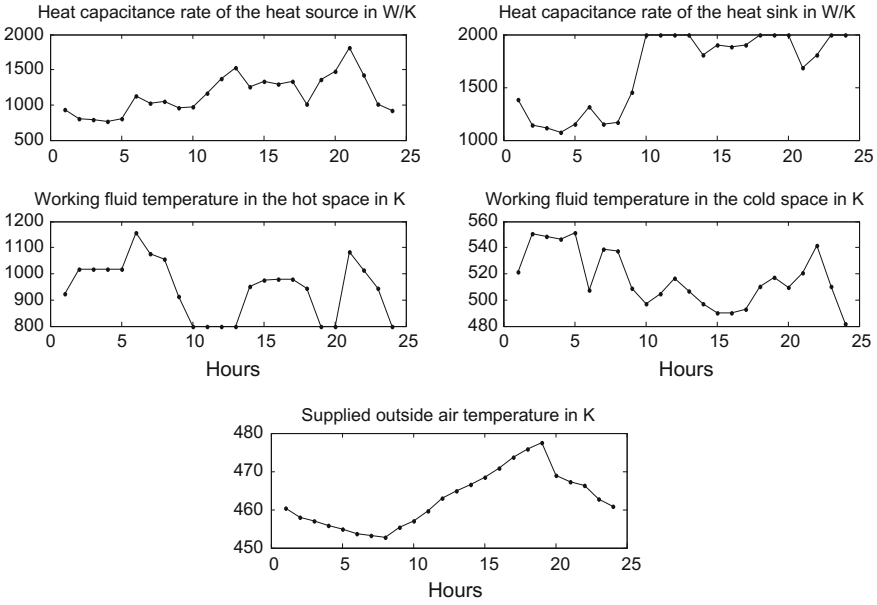

Fig. 15.10 Obtained decision variables in the optimization process of CCP mode

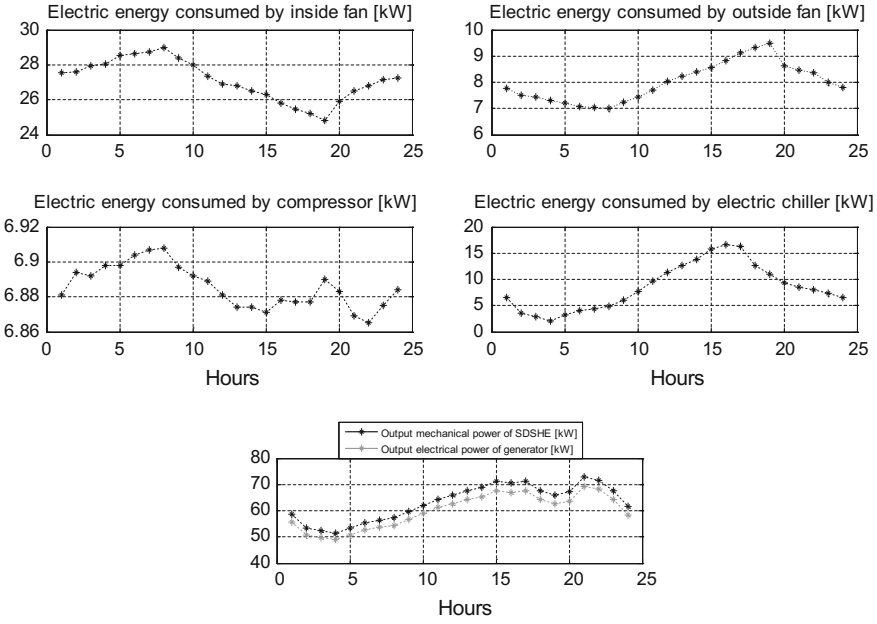

Fig. 15.11 Electric energy consumed by AAHP and electric chiller and generated power during sample summer day in Tabriz, Iran

Table 15.1 Entropy, energy flux between refrigerant and outdoor air, cooling energy generated by AAHP and electric chiller, chilled inside air temperature and exergy flow during sample summer day in Tabriz, Iran

S_{cycle} (kW K^{-1})	S_{evap} (kW K^{-1})		S_{cond} (kW K^{-1})		Q_{cond} (kW)		Q_{evap} (kW)		$T_{out-air_{evap}}$ (K)
0.013	0.095		7.0391E-6		38.660		29.080		292
t (h)	Ex_c (kW)	Ex_{evap} (kW)	$Ex_{out-air_{evap}}$ (kW)	Ex_{in-air} (kW)	Ex_e (kW)	Ex_{cond} (kW)	$Ex_{out-air_{cond}}$ (kW)	Ex_{cycle} (kW)	Q_{EC} (kW)
24–1	1.976	28.611	0.030	0.002	1.100	0.002	9.727	3.805	15.920
1–2	2.171	28.527	0.020	2.464287E−4	0.938	0.002	9.675	3.785	8.920
2–3	2.232	28.819	0.017	0.001	0.882	0.002	9.659	3.779	6.920
3–4	2.329	28.810	0.013	6.543044E−4	0.800	0.002	9.633	3.768	4.920
4–5	2.403	29.255	0.011	0.003	0.734	0.002	9.614	3.761	7.920
5–6	2.500	29.291	0.008	0.003	0.653	0.002	9.588	3.751	9.920
6–7	2.549	29.367	0.007	0.003	0.612	0.002	9.575	3.746	10.920
7–8	2.573	29.555	0.006	0.005	0.592	0.002	9.568	3.743	11.920
8–9	2.378	29.159	0.012	0.003	0.755	0.002	9.620	3.763	14.920
9–10	2.232	28.841	0.017	0.001	0.881	0.002	9.659	3.779	18.920
10–11	2.024	28.393	0.027	3.107073E−4	1.064	0.002	9.714	3.800	23.920
11–12	1.756	28.173	0.043	5.487082E−4	1.297	0.002	9.785	3.828	27.920
12–13	1.610	28.172	0.053	0.001	1.421	0.002	9.824	3.843	30.920
13–14	1.476	27.984	0.063	0.001	1.541	0.002	9.860	3.857	33.920
14–15	1.329	27.893	0.075	0.002	1.669	0.002	9.898	3.872	38.920
15–16	1.134	27.551	0.092	7.347613E−4	1.851	0.002	9.950	3.892	40.920
16–17	0.902	27.390	0.115	0.001	2.058	0.002	10.011	3.916	39.920
17–18	0.732	27.272	0.133	0.002	2.211	0.002	10.057	3.934	30.920
18–19	0.610	26.989	0.147	7.246043E−4	2.333	0.002	10.089	3.947	26.920
19–20	1.281	27.575	0.079	2.405492E−4	1.725	0.002	9.911	3.877	22.920
20–21	1.427	28.043	0.067	0.002	1.580	0.002	9.872	3.862	20.920
21–22	1.500	28.256	0.061	0.003	1.511	0.002	9.853	3.854	19.920
22–23	1.781	28.401	0.041	0.002	1.270	0.002	9.779	3.825	17.920
23–24	1.927	28.378	0.032	6.471150E−4	1.147	0.002	9.740	3.810	15.920

and outside fans, electric chiller and building's electric demand increases. On the other hand, the hourly electrical energy purchased from the local grid during the sample hot day is equal to zero. According to the above results, the AAHP generates 29.080 kW of total cooling energy required for the test residential building. The electric power consumed by the electric chiller and the cooling demand change in a similar manner during the hot day. In the meantime, the minimum and maximum cooling demands are equal to 34 and 70 kW, respectively. Hence, supposing $\dot{m} = 0.2\,\mathrm{kg\,s^{-1}}$ in CCP mode, the AAHP provides almost 41.5% of the total cooling demand during the hottest hour ($t = 16$). If the mass flow rate of the refrigerant increases, the AAHP's thermal capacity and the electric power consumed by the electric chiller will increase and decrease, respectively. Based on Figs. 15.9, 15.10 and 15.11, the electric power consumed by the outside fan, ambient temperature and the supplied outside air temperature change in a similar fashion. According to Eq. (15.24) and assuming that $T_{out-air_{evap}} = 292\,\mathrm{K}$, if the inside air temperature increases, $T_{out-air_{evap}} - T_{in-air}$ becomes more negative. Hence, the electric power consumed by the inside fan will decrease. The electric power consumed by the inside fan maximized and minimized at $t = 8$ and $t = 11$, respectively. These two points coincide with the maximum and minimum points of the inside air temperature. As a result, an air to air heat pump can provide efficient cooling energy for a large-scale residential building using air as a renewable energy source, especially in a warm area. Finally, the cooling distribution systems such as forced air units can distribute the generated cooling energy and the cold weather between different flats and floors.

15.4.2 CHP Mode

The variations of ambient and indoor air temperatures during a sample autumn day are plotted in Fig. 15.12.

The obtained optimum operating points of the proposed tri-generation system in CHP mode can be summarized in Table 15.2 and shown in Figs. 15.13 and 15.14.

According to Figs. 15.8 and 15.14, the mass flow rate of the refrigerant increases monotonically as the value of heating demand increases. Hence, the values of $\dot{m}$ and the maximum and minimum of the heating load occur at $t = 4$ and $t = 15$, respectively. The energy flux between the refrigerant and the outside air will be increased as the values of $\dot{m}$ and heating demand increase. Also, if the heating load increases, the electric energy consumed by the inside fan, required to supply the inside cold weather, will increase. As shown in Fig. 15.14, the sum of the electrical energy consumed by the inside and outside fans, compressor and building's electric demand can be met by generator output power driven by a SDSHE (Thermal storage unit has been used for continuous energy supplying when sunlight is

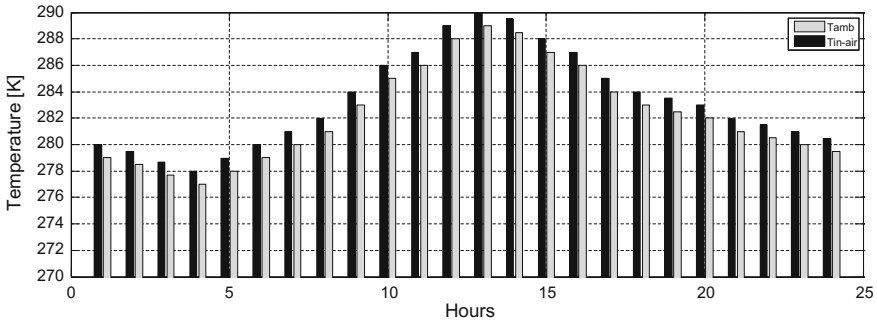

Fig. 15.12 The ambient and indoor air temperatures during an autumn cold day in Tabriz, Iran

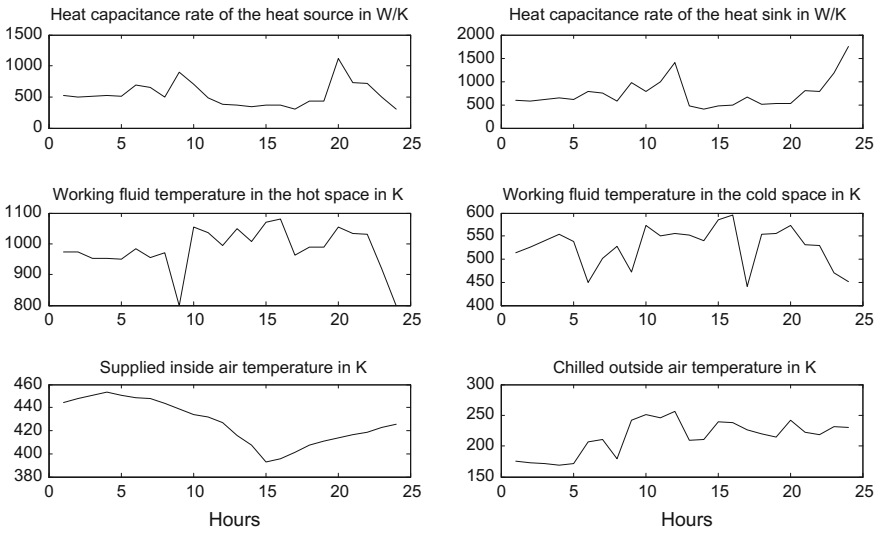

Fig. 15.13 Obtained decision variables in optimization process of CHP mode

insufficient or nighttime). Note that the hourly objective cost obtained from optimizing of CHP mode is zero. From Fig. 15.13, the minimum value of the supplied inside air temperature is equal to 393.12 K. Assuming 10% heat losses in warm air storage tank (WAST), this value is reduced to 353.8080 K. In central heating system, minimum inlet water temperature to radiators is equal to 180 °F or 355.22 K. Hence, the supplied inside air stored in WAST can satisfy the inlet water temperature to radiant floor systems. As an important result, an AAHP can supply

Table 15.2 Exergy flow, entropy, energy flux between refrigerant and outdoor air during sample cold day in Tabriz, Iran

t (h)	Ex_c (kW)	Ex_{evap} (kW)	$Ex_{out-air_{evap}}$ (kW)	Ex_{in-air} (kW)	Ex_e (kW)	Ex_{cond} (kW)	$Ex_{out-air_{cond}}$ (kW)
24–1	4.798	5.914	4.397	0.00033315	3.228	1.676	11.305
1–2	4.972	6.173	4.559	0.00038762	3.306	1.662	11.823
2–3	5.209	6.43	4.715	0.00033471	3.344	1.696	12.338
3–4	5.427	6.692	4.874	0.00033555	3.39	1.706	12.867
4–5	5.168	6.437	4.72	0.00033435	3.382	1.698	12.351
5–6	4.915	13.748	2.159	0.00033315	0.961	1.691	11.844
6–7	4.726	14.049	2.01	0.00033197	0.934	1.691	11.614
7–8	4.429	5.689	4.26	0.00033079	3.326	1.676	10.856
8–9	3.968	18.416	0.069	0.00032846	0	1.66	9.903
9–10	3.532	18.753	0.471	0.00032616	0.004	1.644	8.987
10–11	3.312	16.741	0.647	0.00040116	0.283	1.601	8.543
11–12	2.915	17.463	0.39	0.00039838	0.219	1.585	7.684
12–13	2.555	4.207	2.514	0.00039701	2.436	1.546	6.425
13–14	2.429	2.986	2.432	0.00039769	2.324	1.513	5.624
14–15	2.287	7.784	0.888	0.00039977	0.693	1.459	4.512
15–16	2.461	8.258	0.925	0.00040116	0.655	1.468	4.843
16–17	2.835	7.442	1.33	0.0003273	0.895	1.517	5.536
17–18	3.132	7.503	1.619	0.00032846	1.074	1.54	6.292
18–19	3.276	7.208	1.85	0.00040612	1.247	1.519	6.687
19–20	3.442	14.094	0.668	0.00032962	0.004	1.564	7.093
20–21	3.654	10.427	1.436	0.00033079	0.666	1.572	7.497
21–22	3.808	10.553	1.552	0.00092082	0.67	1.375	7.911
22–23	3.975	14.217	0.974	0.00040974	0.066	1.56	8.364
23–24	4.145	14.72	1.007	0.00041047	0.027	1.571	8.813

(continued)

Table 15.2 (continued)

t (h)	Ex_c (kW)	Ex_{evap} (kW)	$Ex_{out-air_{evap}}$ (kW)	Ex_{in-air} (kW)	Ex_e (kW)	Ex_{cond} (kW)	$Ex_{out-air_{cond}}$ (kW)
t (h)	Ex_{cycle} (kW)	S_{cycle} (kW K^{-1})	S_{evap} (kW K^{-1})	S_{cond} (kW K^{-1})	Q_{evap} (kW)		
24–1	3.743	0.013	0.021	0.006	30.84		
1–2	3.827	0.014	0.022	0.006	31.592		
2–3	3.907	0.014	0.023	0.006	32.345		
3–4	3.988	0.014	0.024	0.006	33.097		
4–5	3.912	0.014	0.023	0.006	32.345		
5–6	3.834	0.014	0.049	0.006	31.592		
6–7	3.802	0.014	0.05	0.006	31.216		
7–8	3.678	0.013	0.02	0.006	30.088		
8–9	3.519	0.012	0.065	0.006	28.584		
9–10	3.357	0.012	0.066	0.006	27.079		
10–11	3.275	0.011	0.059	0.006	26.327		
11–12	3.11	0.011	0.061	0.006	24.823		
12–13	2.837	0.01	0.015	0.005	22.566		
13–14	2.643	0.009	0.01	0.005	21.062		
14–15	2.348	0.008	0.027	0.005	18.805		
15–16	2.433	0.009	0.029	0.005	19.557		
16–17	2.602	0.009	0.026	0.005	21.062		
17–18	2.778	0.01	0.027	0.005	22.566		
18–19	2.866	0.01	0.026	0.005	23.318		
19–20	2.953	0.01	0.05	0.006	24.07		
20–21	3.034	0.011	0.037	0.006	24.823		
21–22	3.115	0.011	0.038	0.005	25.575		
22–23	3.207	0.011	0.051	0.006	26.327		
23–24	3.292	0.012	0.053	0.006	27.079		

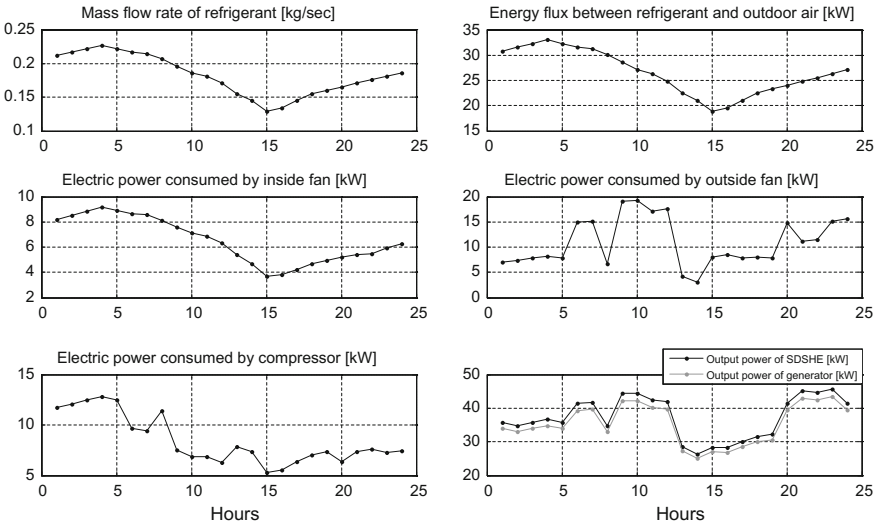

Fig. 15.14 Mass flow rate of refrigerant, energy flux between refrigerant and outdoor air, consumed and generated power during sample cold day in Tabriz, Iran

the total heating demand (Q_{cond}) of large residential towers with different flats and floors during a simple refrigeration cycle using evaporator, compressor, condenser and expansion valve at no cost and without environmental pollutants and greenhouse gas emissions.

15.5 Conclusion

In this chapter, a novel methodology was introduced for short-term scheduling of small-scale tri-generation system, which can be used to provide cooling, heating and power for residential applications. The solar energy may be used as a renewable energy to drive a Stirling engine, which is used to deliver the primary mechanical power required for driving a generator. The heat absorber and thermal storage unit are employed to absorb and store sun radiations collected by the solar dish. The air to air heat pumps were proposed to cool and heat the residential buildings during summer and spring/autumn days, respectively. The proposed micro-CCHP system does not use any fossil fuel such as gasoline and natural gas. Thus, use of solar energy and ASHPs in a CCHP system not only reduces the carbon dioxide, greenhouse gas emissions and environmental pollution, but also reduces the fuel consumption. Meanwhile, the proposed CCHP microgrid consumes less electricity energy than the traditional tri-generation systems. The contributions of the current chapter can be summarized as follows:

- Environmental friendliness: In this chapter, solar energy and air are used as renewable energy sources to drive a prime mover and an air to air heat pump, which is required in order to provide mechanical and cooling/heating energies for a modern residential tower.
- Cost-cutting: The air to air heat pump was proposed to cool and heat the residential buildings in CCP and CHP modes. The energy required to operate the refrigeration cycle is the electrical energy, which powers the compressor, inside and outside fans. Hence, AAHPs based CCHP consumes less electrical energy than the traditional fossil fuels-based tri-generation systems.
- On-site fulfillment: The heating energy obtained from ASHPs is not generated by a combustion process, but is transferred from one place to another.

It is clear that building's insulation reduces heat losses and can decrease the heating and the cooling demands. Hence, the electrical energy consumed by AAHP and electric chiller will be reduced. In a nutshell, a novel zero energy system was proposed to make residential tower technology smarter.

Appendix

The specifications of the solar powered Stirling engine are considered as follows [25, 28]:

$I = 1000\,\mathrm{Wm^{-2}}$, $C = 1300$, $\varepsilon = 0.9$, $\eta_0 = 0.9$, $K_0 = 2.5\,\mathrm{WK^{-1}}$, $n = 1$, $C_v = 15\,\mathrm{J\,mol^{-1}\,K^{-1}}$, $R = 4.3\,\mathrm{J\,mol^{-1}\,K^{-1}}$, $T_{H_1} = 1300\,\mathrm{K}$, $T_{L_1} = 290\,\mathrm{K}$, $\xi = 2 \times 10^{-10}$, $h = 20\,\mathrm{Wm^{-2}K^{-1}}$, $\lambda = 2$, $1/M_1 + 1/M_2 = 2 \times 10^{-5}\,\mathrm{sK^{-1}}$, $\delta = 5.67 \times 10^{-8}\,\mathrm{Wm^{-2}K^{-4}}$, $\varepsilon_H = \varepsilon_L = \varepsilon_R = 0.9$,$\eta_{elec} = 0.95$

The electricity energy price at each hour has been reported in Table 15.3 [28].

The specification of the AAHP's refrigeration cycle and the electric chiller's COP are given as follows [29]:

$P_1 = 100\,\mathrm{kPa}$, $P_2 = 800\,\mathrm{kPa}$, $T_1 = -20\,^{\circ}\mathrm{C}$, $T_2 = 50\,^{\circ}\mathrm{C}$, $T_3 = 30\,^{\circ}\mathrm{C}$, $T_4 = -25\,^{\circ}\mathrm{C}$, $h_1 = 387.2\,\mathrm{kJ\,kg^{-1}}$, $h_2 = 435.1\,\mathrm{kJ\,kg^{-1}}$ $h_3 = h_4 = 241.8\,\mathrm{kJ\,kg^{-1}}$, Energy requirement of electric chiller $= 0.7\,\mathrm{kWton^{-1}}$, $COP = 2.46$, $C_a = 1.15\,\mathrm{kJ\ kg^{-1}K^{-1}}$, $m_{in-air} = 0.2\,\mathrm{kg\,s^{-1}}$, $m_{out-air} = 0.2\,\mathrm{kg\,s^{-1}}$, $\dot{m} = 0.2\,\mathrm{kg\,s^{-1}}$ for CCP mode, $T_C = 317\,\mathrm{K}$, $T_e = 290\,\mathrm{K}$

Table 15.3 Hourly electricity price

t (h)	24–1	1–2	2–3	3–4	4–5	5–6	6–7	7–8
λ_t ($/kWh)	0.068	0.090	0.093	0.095	0.097	0.099	0.098	0.096
t (h)	8–9	9–10	10–11	11–12	12–13	13–14	14–15	15–16
λ_t ($/kWh)	0.095	0.092	0.094	0.097	0.100	0.120	0.103	0.099
t [hour]	16–17	17–18	18–19	19–20	20–21	21–22	22–23	23–24
λ_t ($/kWh)	0.085	0.078	0.075	0.084	0.096	0.081	0.067	0.063

Table 15.4 The specifications of the test building [28]

Building type	Residential
Number of floors	6
Number of flats	12
Total effective floor area in m^2	1080
Average ceiling height in m	3

Table 15.5 Equipment cost of proposed tri-generation system's components

Equipment	Cost ($)	Equipment	Cost ($)
Solar dish Stirling heat engine	12680	Condenser	6280
Thermal storage tank	4400	Evaporator	9600
Power generation unit	3015	Compressor	7700
Electric chiller	585	Expansion device	600
Inside fan	450	Warm air storage tank	7600
Outside fan	725		

In this chapter, a benchmark residential building with 1080 m^2 area is assumed in Tabriz, Iran to be delivered cool, heat and power by the proposed micro-trigeneration system. The specifications of the benchmark building are reported in Table 15.4.

Equipment cost of proposed micro-CCHP system's components has been reported in Table 15.5.

References

1. Liu M, Shi Y, Fang F (2012) A new operation strategy for CCHP systems with hybrid chillers. Appl Energy 95:164–173. doi:10.1016/j.apenergy.2012.02.035
2. Wang M, Wang J, Zhao P, Dai Y (2015) Multi-objective optimization of a combined cooling, heating and power system driven by solar energy. Energy Convers Manag 89:289–297. doi:10.1016/j.enconman.2014.10.009
3. Guo L, Liu W, Cai J, Hong B, Wang C (2013) A two-stage optimal planning and design method for combined cooling, heat and power microgrid system. Energy Convers Manag 74:433–445. doi:10.1016/j.enconman.2013.06.051
4. Ghaebi H, Saidi MH, Ahmadi P (2012) Exergoeconomic optimization of a trigeneration system for heating, cooling and power production purpose based on TRR method and using evolutionary algorithm. Appl Therm Eng 36:113–125. doi:10.1016/j.applthermaleng.2011.11.069
5. Al-Sulaiman FA, Dincer I, Hamdullahpur F (2011) Exergy modeling of a new solar driven trigeneration system. Sol Energy 85(9):2228–2243. doi:10.1016/j.solener.2011.06.009
6. Gharieh K, Jafari MA, Guo Q (2015) Investment in hydrogen tri-generation for wastewater treatment plants under uncertainties. J Power Sourc 297:302–314. doi:10.1016/j.jpowsour.2015.07.093
7. Ebrahimi M, Keshavarz A (2012) Prime mover selection for a residential micro-CCHP by using two multi-criteria decision-making methods. Energy Build 55:322–331

8. Intini M, De Antonellis S, Joppolo CM, Casalegno A (2015) A trigeneration system based on polymer electrolyte fuel cell and desiccant wheel—Part B: overall system design and energy performance analysis. Energy Convers Manag 106:1460–1470. doi:10.1016/j.enconman.2015.10.005
9. Zhao H, Jiang T, Hou H (2015) Performance analysis of the SOFC–CCHP system based on H2O/Li–Br absorption refrigeration cycle fueled by coke oven gas. Energy 91:983–993. doi:10.1016/j.energy.2015.08.087
10. Wang JL, Wu JY, Zheng CY (2014) Simulation and evaluation of a CCHP system with exhaust gas deep-recovery and thermoelectric generator. Energy Convers Manag 86:992–1000. doi:10.1016/j.enconman.2014.06.036
11. Boyaghchi FA, Heidarnejad P (2015) Thermoeconomic assessment and multi objective optimization of a solar micro CCHP based on Organic Rankine Cycle for domestic application. Energy Convers Manag 97:224–234. doi:10.1016/j.enconman.2015.03.036
12. Liu W, Chen G, Yan B, Zhou Z, Du H, Zuo J (2015) Hourly operation strategy of a CCHP system with GSHP and thermal energy storage (TES) under variable loads: a case study. Energy Build 93:143–153. doi:10.1016/j.enbuild.2015.02.030
13. Wang J-J, Yang K, Xu Z-L, Fu C (2015) Energy and exergy analyses of an integrated CCHP system with biomass air gasification. Appl Energy 142:317–327. doi:10.1016/j.apenergy.2014.12.085
14. Jannelli E, Minutillo M, Cozzolino R, Falcucci G (2014) Thermodynamic performance assessment of a small size CCHP (combined cooling heating and power) system with numerical models. Energy 65:240–249. doi:10.1016/j.energy.2013.11.074
15. Rey G, Ulloa C, Cacabelos A, Barragáns B (2015) Performance analysis, model development and validation with experimental data of an ICE-based micro-CCHP system. Appl Therm Eng 76:233–244. doi:10.1016/j.applthermaleng.2014.10.087
16. Li L, Mu H, Gao W, Li M (2014) Optimization and analysis of CCHP system based on energy loads coupling of residential and office buildings. Appl Energy 136:206–216. doi:10.1016/j.apenergy.2014.09.020
17. Wu JY, Wang JL, Li S, Wang RZ (2014) Experimental and simulative investigation of a micro-CCHP (micro combined cooling, heating and power) system with thermal management controller. Energy 68:444–453. doi:10.1016/j.energy.2014.02.057
18. Jabbari B, Tahouni N, Ataei A, Panjeshahi MH (2013) Design and optimization of CCHP system incorporated into kraft process, using Pinch Analysis with pressure drop consideration. Appl Therm Eng 61(1):88–97. doi:10.1016/j.applthermaleng.2013.01.050
19. Andiappan V, Tan RR, Aviso KB, Ng DKS (2015) Synthesis and optimisation of biomass-based tri-generation systems with reliability aspects. Energy 89:803–818. doi:10.1016/j.energy.2015.05.138
20. Tippawan P, Arpornwichanop A, Dincer I (2015) Energy and exergy analyses of an ethanol-fueled solid oxide fuel cell for a trigeneration system. Energy 87:228–239. doi:10.1016/j.energy.2015.04.072
21. Dominković DF, Ćosić B, Bačelić Medić Z, Duić N (2015) A hybrid optimization model of biomass trigeneration system combined with pit thermal energy storage. Energy Convers Manag 104:90–99. doi:10.1016/j.enconman.2015.03.056
22. Ozcan H, Dincer I (2014) Thermodynamic analysis of a combined chemical looping-based trigeneration system. Energy Convers Manag 85:477–487
23. Soroudi A, Mohammadi-Ivatloo B, Rabiee A (2014) Energy hub management with intermittent wind power. In: Large scale renewable power generation. Springer, pp 413–438
24. Mohammadi-Ivatloo B, Moradi-Dalvand M, Rabiee A (2013) Combined heat and power economic dispatch problem solution using particle swarm optimization with time varying acceleration coefficients. Electr Power Syst Res 95:9–18
25. Yaqi L, Yaling H, Weiwei W (2011) Optimization of solar-powered Stirling heat engine with finite-time thermodynamics. Renew Energy 36(1):421–427
26. Turner LW (1979) Heat pumps for residential heating and cooling: some questions and answers. Michigan State University Energy for Agriculture Series ENR, USA, No 80–35

27. Karami R, Sayyaadi H (2015) Optimal sizing of Stirling-CCHP systems for residential buildings at diverse climatic conditions. Appl Therm Eng 89:377–393. doi:10.1016/j.applthermaleng.2015.06.022
28. Kaushik SC, Kumar S (2001) Finite time thermodynamic evaluation of irreversible Ericsson and Stirling heat engines. Energy Convers Manag 42(3):295–312. doi:10.1016/S0196-8904(00)00063-7
29. Sonntag RE, Borgnakke C, Van Wylen GJ, Van Wyk S (1998) Fundamentals of thermodynamics, vol 6. Wiley, New York